

Visual Motion Observer-based Stabilizing Receding Horizon Control via Obstacle Avoidance Navigation Function

Toshiyuki Murao, Hiroyuki Kawai and Masayuki Fujita

Abstract—This paper investigates stabilizing receding horizon control via an obstacle avoidance navigation function for three-dimensional (3-D) eye-to-hand visual feedback systems. Firstly, a visual motion observer for a controlled mobile robot is presented. Then, visual motion observer-based stabilizing receding horizon control for 3-D visual feedback systems, highly nonlinear and relatively fast systems, is proposed. Moreover, a path planner to be appropriate for the visual motion error system is designed through an obstacle avoidance navigation function to keep collision-free during servoing. Finally, the effectiveness of the proposed method is verified through computer simulations.

I. INTRODUCTION

Visual feedback control, which can be regarded as a cross-point between control theory and computer vision, is now a very flexible and useful method in robot control [1]. Recently, Lippiello *et al.* [2] presented position-based visual servoing for hybrid eye-in-hand/eye-to-hand multicamera systems by using an extended Kalman filter and a multi-arm robotic cell. Gans and Hutchinson [3] proposed hybrid switched-system control which incorporates both an image-based visual servoing controller and a position-based one. Swensen *et al.* [4] presented featureless kernel-based visual servoing and discussed a domain of attraction of the method through experiments. Allibert *et al.* [5] reported comparison results between two image prediction models for an image-based visual servoing scheme based on nonlinear model predictive control. Gans *et al.* [6] proposed a method which regulates functions of the current image features without the need of a goal image or a goal feature trajectory. The authors have been proposed passivity-based visual feedback control for three-dimensional (3-D) target tracking in a series of papers [7]–[9].

On the other hand, obstacle avoidance coupled with accurate path following control which is to move a vehicle towards a target location free of collisions with the obstacles has attracted much attention of a great amount of robotics researchers [10]. One of the representative works for obstacle avoidance problems is a method using a navigation function that is globally convergent potential function proposed by Rimon and Koditschek [11]. The feature of this efficient

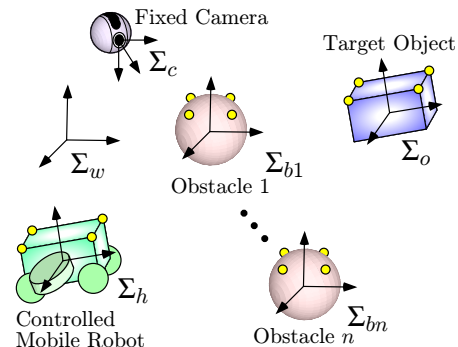


Fig. 1. Eye-to-hand visual feedback system with obstacles.

approach is that automatically merge path finding and trajectory generation in a closed-loop fashion. Some navigation function approaches for visual feedback systems are reported in [12]–[14]. Cowan *et al.* [12] proposed a visual feedback controller to bring a robot to rest at a desired configuration keeping all feature points within a camera field of view by using navigation functions. Chen *et al.* [13] and the authors [14] developed an off-line path planner based on an image space navigation function with an adaptive 2 1/2-D visual servoing controller and a stabilizing receding horizon one, respectively. However, all these approaches [12]–[14] take advantage of navigation functions to solve the camera field of view problems but not to deal with the obstacle avoidance problems.

Among the different proposals from the navigation function approach, a number of navigation strategies for obstacle avoidance in conjunction with visual information has been reported. Huang *et al.* [15] presented a local navigation method with a single camera for obstacle avoidance using headings to obstacles and their angular widths. Cherubini and Chaumette [16] proposed appearance-based visual navigation with obstacle avoidance for real outdoor environments. This appearance-based visual navigation, which is one of the few methods for obstacle avoidance through the camera model, avoids new obstacles by using a range scanner. Although good vision-based navigation approaches for the obstacle avoidance problems are presented in [15] and [16], they are restricted to a ground vehicle. Moreover, the desired control performance cannot be guaranteed explicitly, since these control methods are not based on optimal control theory.

In this paper, stabilizing receding horizon control via a navigation function for obstacle avoidance is applied to 3-D visual feedback systems with an eye-to-hand configuration as shown in Fig. 1, highly nonlinear and relatively fast systems. Firstly, a visual motion observer for a controlled

This work was not supported by any organization

T. Murao is with Master Program of Innovation for Design and Engineering Advanced Institute of Industrial Technology, Tokyo 140-0011, Japan murao-toshiyuki@aait.ac.jp

H. Kawai is with Department of Robotics, Kanazawa Institute of Technology, Ishikawa 921-8501, Japan

M. Fujita is with Department of Mechanical and Control Engineering, Tokyo Institute of Technology, Tokyo 152-8550, Japan

mobile robot is constructed. Secondly, stabilizing receding horizon control for a visual motion error system using a control Lyapunov function is proposed. Then, a path planner to be appropriate for the visual motion error system is designed through an obstacle avoidance navigation function in order to move the robot towards a desired pose and away from obstacles without additional sensors such as a range scanner. Convergence analysis of the proposed path planner is provided. Finally, control performance of the proposed control scheme with obstacle avoidance and the previous one [9] is evaluated through simulation results.

II. VISUAL MOTION OBSERVER FOR CONTROLLED MOBILE ROBOT

The section II-A and II-B mainly reviews our previous work [7] via the passivity-based visual feedback control.

A. Vision Camera Model

Eye-to-hand visual feedback systems with obstacles use four and n coordinate frames which consist of a world frame Σ_w , a fixed camera frame Σ_c , a mobile robot frame Σ_h , a target object frame Σ_o and n obstacle frames $\Sigma_{b_1}, \dots, \Sigma_{b_n}$ as depicted in Fig. 1. Let $p_{ho} \in \mathcal{R}^3$ and $e^{\hat{\xi}\theta_{ho}} \in SO(3)$ be a position vector and a rotation matrix from the mobile robot frame Σ_h to the target object frame Σ_o . Then, a relative pose from Σ_h to Σ_o can be represented by $g_{ho} = (p_{ho}, e^{\hat{\xi}\theta_{ho}}) \in SE(3)$.

The objective of position-based visual feedback control is, in general, to bring the relative pose g_{ho} to a final reference one g_{hod_f} . The relative pose g_{ho} can be represented by using the composition rule for rigid body transformations [17] as follows:

$$g_{ho} = g_{ch}^{-1} g_{co}. \quad (1)$$

The relative poses g_{ch} and g_{co} can be led using poses under the world frame Σ_w as

$$g_{ch} = g_{wc}^{-1} g_{wh}, \quad g_{co} = g_{wc}^{-1} g_{wo}. \quad (2)$$

The relative pose involves a velocity of each rigid body. We define a body velocity of the mobile robot relative to the world frame Σ_w as $V_{wh}^b = [(v_{wh}^b)^T (\omega_{wh}^b)^T]^T$, where v_{wh}^b and ω_{wh}^b represent a velocity of an origin and an angular velocity from Σ_w to Σ_h , respectively [17]. Differentiating Eq. (2) with respect to time, the body velocities of the relative poses g_{ch} and g_{co} can be written as follows (See [8]):

$$V_{ch}^b = V_{wh}^b, \quad V_{co}^b = V_{wo}^b, \quad (3)$$

where V_{wo}^b is the body velocity of the target object relative to Σ_w . Here, we exploit the property of the eye-to-hand visual feedback system whose camera is fixed in the environment.

In this visual feedback system, we use a pinhole camera model with a perspective projection. Here, we consider $m(\geq 4)$ feature points on the rigid mobile robot and target object in this paper. Let λ be a focal length, $p_{ai} \in \mathcal{R}^3$ and $p_{ci} \in \mathcal{R}^3$ be the position vectors of the i -th feature point relative to Σ_o and Σ_c , respectively. Here, we represent each observed frame (i.e., Σ_h or Σ_o) as Σ_a . Using a transformation of the coordinates, we have $p_{cai} = g_{ca} p_{ai}$, where p_{cai} and

p_{ai} should be regarded, with a slight abuse of notation, as $[p_{cai}^T \ 1]^T$ and $[p_{ai}^T \ 1]^T$. We assume that the position of multiple points on the mobile robot p_{hi} and that on the target object p_{oi} are given. The perspective projection of the i -th feature point onto the image plane gives us the image plane coordinate $f_{cai} := [f_{cai x} \ f_{cai y}]^T \in \mathcal{R}^2$ as

$$f_{cai} = \frac{\lambda}{z_{cai}} \begin{bmatrix} x_{cai} \\ y_{cai} \end{bmatrix}, \quad (4)$$

where $p_{cai} = [x_{cai} \ y_{cai} \ z_{cai}]^T$. It is straightforward to extend this model to m image points by simply stacking the vectors of the image plane coordinate, i.e., $f(g_{ca}) := [f_{ca1}^T \ \dots \ f_{cam}^T]^T \in \mathcal{R}^{2m}$. Hereafter, f_{ca} means $f(g_{ca})$ for simplicity. The image features f_{ch} and f_{co} only depend on the relative poses g_{ch} and g_{co} , respectively.

B. Estimation Error System for Target Object

In this subsection, we consider a nonlinear observer (we call a visual motion observer) for the target object in order to estimate the relative pose g_{co} from the image feature f_{co} . Using the body velocity of the relative pose g_{co} (3), we choose estimates $\bar{g}_{co} = (\bar{p}_{co}, e^{\hat{\xi}\bar{\theta}_{co}})$ and \bar{V}_{co}^b of the relative pose and velocity, respectively as

$$\bar{V}_{co}^b = u_o. \quad (5)$$

The new input u_o is to be determined in order to drive the estimated values \bar{g}_{co} and \bar{V}_{co}^b to their actual values.

In order to establish an estimation error system, we define an estimation error for the target object between the estimated value \bar{g}_{co} and the actual relative pose g_{co} as

$$e_o = \bar{g}_{co}^{-1} g_{co}. \quad (6)$$

We next define an error vector of the rotation matrix $e^{\hat{\xi}\theta_{ei}}$ as $r_{ei} := \text{sk}(e^{\hat{\xi}\theta_{ei}})^\vee$ where $\text{sk}(e^{\hat{\xi}\theta_{ei}})$ denotes $\frac{1}{2}(e^{\hat{\xi}\theta_{ei}} - e^{-\hat{\xi}\theta_{ei}})$. Using this notation, the vector of the estimation error for the target object is given by $e_o := [p_{eo}^T \ r_{eo}^T]^T$. Suppose an attitude estimation error θ_{eo} is small enough that we can let $e^{\hat{\xi}\theta_{eo}} \simeq I + \text{sk}(e^{\hat{\xi}\theta_{eo}})$. Therefore, using a first-order Taylor expansion approximation, the estimation error vector e_o can be obtained from the image feature f_{co} and the estimated value of the relative pose \bar{g}_{co} (i.e., the measurement and the estimate) as follows:

$$e_o = J^\dagger(\bar{g}_{co})(f_{co} - \bar{f}_{co}), \quad (7)$$

where \bar{f}_{co} is an estimated value of the image feature and $J(\bar{g}_{co})$ is an image Jacobian-like matrix [8]. In the same way as Eq. (3), the estimation error system for the target object can be represented by

$$V_{eo}^b = -\text{Ad}_{(g_{eo}^{-1})} u_o + V_{wo}^b. \quad (8)$$

C. Estimation Error System for Controlled Mobile Robot

In our previous work [7], we constructed the visual motion observer for the mobile robot, which estimates the relative pose g_{ch} from the image feature f_{ch} , using the same dynamical model as the visual motion observer for the target object, i.e., $\bar{V}_{ch}^b = u_{eh}$. However, the estimation input u_{eh} has directly affected not only estimation but also control;

as a result, this leads to degraded estimation performance from the practical viewpoint. In order to remove the above negative effect in this paper, we design a novel visual motion observer to embed the input of the controlled mobile robot.

Firstly, we define the estimation error for the controlled mobile robot between the relative pose g_{ch} and the estimated value \bar{g}_{ch} as

$$g_{eh} = \bar{g}_{ch}^{-1} g_{ch}. \quad (9)$$

The vector of the estimation error for the controlled mobile robot is also represented as $e_h := [p_{eh}^T \ r_{eh}^T]^T$. It should be noted that this estimation error vector e_h can be calculated as

$$e_h = J^\dagger(\bar{g}_{ch})(f_{ch} - \bar{f}_{ch}), \quad (10)$$

where \bar{f}_{ch} is an estimated value of the image feature f_{ch} .

Next, we consider the following dynamical model in order to estimate the controlled mobile robot:

$$\dot{V}_{ch}^b = \text{Ad}_{(g_{eh})} V_{wh}^b + u_h. \quad (11)$$

Here, the estimation error matrix g_{eh} is extracted using the estimation error vector e_h in Sec III. Also, the new input u_h is designed in the next section. The visual motion observer for the target object cannot embed the body velocity V_{wo}^b because the movement of the target object is unknown information. On the other hand, the input of the controlled mobile robot V_{wh}^b can be utilized to the visual motion observer as Eq. (11).

Differentiating Eq. (9) with respect to time, the estimation error system for the controlled mobile robot can be represented by

$$\dot{V}_{eh}^b = -\text{Ad}_{(g_{eh}^{-1})} u_h. \quad (12)$$

III. VISUAL MOTION OBSERVER-BASED STABILIZING RECEDING HORIZON CONTROL

A. Pose Control Error System

Let us consider the dual of the estimation error system in order to achieve the control objective. We define the pose control error as follows:

$$g_{ec} = g_{hod}^{-1} g_{ho}, \quad (13)$$

which represents the error between the relative pose g_{ho} and the reference one g_{hod} . It should be remarked that the relative pose g_{ho} can be calculated by using the estimated relative poses \bar{g}_{ch} and \bar{g}_{co} and the estimation error vectors $e_h = [p_{eh}^T \ r_{eh}^T]^T$ and $e_o = [p_{eo}^T \ r_{eo}^T]^T$ equivalently as follows:

$$g_{ho} = g_{eh}^{-1} \bar{g}_{ch}^{-1} \bar{g}_{co} g_{eo} \quad (14)$$

$$\xi\theta_{eh} = \frac{\sin^{-1} \|r_{eh}\|}{\|r_{eh}\|} r_{eh}, \quad \xi\theta_{eo} = \frac{\sin^{-1} \|r_{eo}\|}{\|r_{eo}\|} r_{eo}, \quad (15)$$

although g_{ho} cannot be measured directly (see [9] for more details). It should be noted that the estimation matrix g_{eh} is calculated in this process. Similar to the estimation error vectors, the vector of the pose control error is defined as $e_c := [p_{ec}^T \ r_{ec}^T]^T$.

Differentiating Eq. (13) with respect to time, the pose control error system can be represented as

$$\dot{V}_{ec}^b = -\text{Ad}_{(g_{ec}^{-1})} \left(\text{Ad}_{(g_{hod}^{-1})} V_{wh}^b + V_{hod}^b \right) + V_{wo}^b, \quad (16)$$

where V_{hod}^b is the body velocity of the reference of the relative pose g_{hod} .

B. Passivity of Visual Motion Error System

Combining the estimation error systems (8) (12) and the pose control one (16), we construct the visual motion observer-based pose control error system (we call the visual motion error system) as follows:

$$\begin{bmatrix} \dot{V}_{ec}^b \\ \dot{V}_{eh}^b \\ \dot{V}_{eo}^b \end{bmatrix} = \begin{bmatrix} -\text{Ad}_{(g_{ec}^{-1})} & 0 & 0 \\ 0 & -\text{Ad}_{(g_{eh}^{-1})} & 0 \\ 0 & 0 & -\text{Ad}_{(g_{eo}^{-1})} \end{bmatrix} u + \begin{bmatrix} I \\ 0 \\ I \end{bmatrix} V_{wo}^b, \quad (17)$$

where

$$u := [u_c^T \ u_h^T \ u_o^T]^T, \quad u_c := \text{Ad}_{(g_{hod}^{-1})} V_{wh}^b + V_{hod}^b. \quad (18)$$

Let us define the error vector of the visual motion error system as $x := [e_c^T \ e_h^T \ e_o^T]^T$ which consists of the pose control error vector e_c and the estimation error vectors e_h and e_o . It should be noted that if the vectors of the pose control error and the estimation ones are equal to zero, then the actual relative pose g_{ho} tends to the reference one g_{hod} when $x \rightarrow 0$.

The visual motion error system (17) has important relation between the input and the output.

Lemma 1: If $V_{wo}^b = 0$, then the visual motion error system (17) satisfies

$$\int_0^T u^T(-x) dt \geq -\beta, \quad \forall T > 0 \quad (19)$$

where β is a positive scalar.

The Lemma 1 can be proved by using the following positive definite function:

$$V = E(g_{ec}) + E(g_{eh}) + E(g_{eo}), \quad (20)$$

where $E(g_{ei}) := \frac{1}{2} \|p_{ei}\|^2 + \phi(e^{\xi\theta_{ei}})$ and $\phi(e^{\xi\theta_{ei}}) := \frac{1}{2} \text{tr}(I - e^{\xi\theta_{ei}})$ is an error function of the rotation matrix.

C. Visual Motion Observer-based Stabilizing Receding Horizon Control

In this subsection, the finite horizon optimal control problem (FHOCP) for the visual motion error system (17) is considered. The FHOCP for the system (17) at time t consists of the minimization with respect to the input $u(\tau, x(\tau))$, $\tau \in [t, t+T]$, of the following cost function

$$J(x_0, u, T) = \int_t^{t+T} l(x(\tau), u(\tau)) d\tau + F(x(t+T)) \quad (21)$$

$$l(x(t), u(t)) = E_{qc}(g_{ec}(t)) + E_{qh}(g_{eh}(t)) + E_{qo}(g_{eo}(t)) + u^T(t) R(t) u(t) \quad (22)$$

$$F(x) = \rho V(x) \quad (23)$$

$$q_{pi}(t) \geq 0, \quad q_{Ri}(t) \geq 0, \quad \rho > 0,$$

where $R(t)$ is a positive diagonal matrix, and $E_{qi}(g_{ei}(t)) := q_{pi}(t) \|p_{ei}(t)\|^2 + q_{Ri}(t) \phi(e^{\xi\theta_{ei}(t)})$ ($i \in c, h, o$), with the state $x(t) = x_0$. The speciality of the cost function (21)–(23) is that the terminal cost is derived from the energy function of the visual motion error system. Furthermore, the rotation error related part of the stage cost is derived from the error

function $\phi(e^{\hat{\xi}\theta_{ab}})$ instead of the commonly used quadratic form $\|r_{ab}\|^2$. For a given initial condition x_0 , we denote this solution of the FHOC as $u^*(\tau, x(\tau))$, $\tau \in [t, t + T]$. In receding horizon control, at each sampling time δ , the resulting feedback control at state x_0 is obtained by solving the FHOC and setting

$$u = u^*(\delta, x_0). \quad (24)$$

Suppose that the target object is static, the following theorem concerning the convergence of the stabilizing receding horizon control for the visual motion error system.

Theorem 1: Consider the cost function (21)–(23) for the visual motion error system (17). Suppose that $V_{wo}^b = 0$, $\|\theta_{ec}\| \leq \frac{\pi}{2}$, $\|\theta_{eh}\| \leq \frac{\pi}{2}$, $\|\theta_{eo}\| \leq \frac{\pi}{2}$, and $\rho^2 I \geq 4QR$, then the receding horizon control for the visual motion error system is asymptotically stabilizing.

Theorem 1 concerning stability of the receding horizon control can be proved by using the control Lyapunov function for the 3-D visual motion error system (17) similar to [9]. Since the stabilizing receding horizon control design is based on optimal control theory, the control performance should be improved under the condition of adequate gain assignment in the cost function.

Remark 1: One of the contributions in this paper is that the proposed control law can be applied to the 3-D eye-to-hand visual feedback systems with the mobile robot, because the visual motion error system is combined with the visual motion observer for the controlled mobile robot unlike [9].

IV. OBSTACLE AVOIDANCE NAVIGATION FUNCTION-BASED PATH PLANNING

Vision-based navigation with obstacle avoidance should offer great perspectives in many applications, such as surveillance, patrolling, search and rescue or high risk missions. However, few results have been applied to the full 3-D visual feedback system that includes the camera model with the perspective projection. In this section, as a first step for a vision-based navigation, we design a path planner through an obstacle avoidance navigation function for 3-D eye-to-hand visual feedback systems. The control objective in this paper is stated as follows:

Control Objective: The mobile robot follows the target object, i.e., the relative pose $g_{ho}(t)$ is coincided with the time-varying desired one $g_{hod}(t)$ which is generated to avoid unexpected obstacles, and which converges the final desired one g_{hod_f} .

From the proposed stabilizing receding horizon control law for the visual motion error system, the input to the mobile robot is designed as follows:

$$V_{wh}^b = \text{Ad}_{(g_{hod})} (u_c - V_{hod}^b). \quad (25)$$

Hence, the mobile robot input is needed the body velocity $V_{hod}^b = [(v_{hod}^b)^T (\omega_{hod}^b)^T]^T$ of the reference of the relative pose g_{hod}^1 .

¹The relative pose g_{hod} can be obtained solving $\dot{g}_{hod} = g_{hod} \hat{V}_{hod}^b$.

A. Rotation Error for Path Planning

In rotation control, we consider only convergence to the final desired rotation. We define the rotation error between the time-varying relative desired rotation $e^{\hat{\xi}\theta_{hod}}$ and the final one $e^{\hat{\xi}\theta_{hod_f}}$ as follows:

$$e^{\hat{\xi}\theta_{ed}} = e^{-\hat{\xi}\theta_{hod_f}} e^{\hat{\xi}\theta_{hod}}. \quad (26)$$

The vector form is defined as $r_{ed} := \text{sk}(e^{\hat{\xi}\theta_{ed}})$. Differentiating Eq. (26) with respect to time, the rotation error system for path planning can be written as

$$\omega_{ed}^b = \omega_{hod}^b. \quad (27)$$

B. Visual Motion Observer for Path Planning

Obstacle avoidance navigation function-based path planning needs the relative position of the obstacles from the camera frame p_{cb_i} . In this section, we design the visual motion observer in order to estimate the relative position p_{cb_i} using the image feature $f_{cb_i} := f(g_{cb_i})$. Now, we assume that the camera can observe the multiple points on the obstacles and the position of them p_{bi} is known, similar to the case of the target object and the controlled mobile robot. The body velocity of the relative pose g_{cb_i} can be written as follows:

$$V_{cb_i}^b = -\text{Ad}_{(g_{cb_i}^{-1})} V_{wc}^b + V_{wb_i}^b, \quad (28)$$

where $V_{wb_i}^b$ is the i -th obstacle body velocity. Using the body velocity $V_{cb_i}^b$ (28), we establish a following estimate model for the obstacles:

$$\bar{V}_{cb_i}^b = -\text{Ad}_{(\bar{g}_{cb_i}^{-1})} V_{wc}^b + u_{b_i}, \quad (29)$$

where \bar{g}_{cb_i} and $\bar{V}_{cb_i}^b$ are the estimated values of g_{cb_i} and $V_{cb_i}^b$, respectively. We define the estimation error for the obstacles g_{eb_i} between the actual relative pose g_{cb_i} and the estimated one \bar{g}_{cb_i} as follows:

$$g_{eb_i} = \bar{g}_{cb_i}^{-1} g_{cb_i}. \quad (30)$$

The vector of the estimation error for the obstacles $e_{b_i} = [p_{eb_i}^T \ r_{eb_i}^T]^T$ can be obtained by exploiting the image feature f_{cb_i} and the estimate values \bar{g}_{cb_i} and \bar{f}_{cb_i} as

$$e_{b_i} = J_e^{\dagger}(\bar{g}_{cb_i})(f_{cb_i} - \bar{f}_{cb_i}). \quad (31)$$

Hence, the relative position p_{cb_i} can be calculated as follows:

$$p_{cb_i} = e^{\hat{\xi}\bar{\theta}_{cb_i}} p_{eb_i} + \bar{p}_{cb_i} \quad (32)$$

through $g_{cb_i} = \bar{g}_{cb_i} g_{eb_i}$. The estimation error system for the obstacles can be obtained as

$$V_{eb_i}^b = -\text{Ad}_{(g_{eb_i}^{-1})} u_{b_i} + V_{wb_i}^b. \quad (33)$$

C. Obstacle Avoidance Navigation Function

In this subsection, we develop the obstacle avoidance navigation function $\varphi(p_{chd})$ [11], [18]. In this paper, we assume that the workspace and the obstacles are spherical. This assumption does not constrain the generality of this work since it has been proven that navigation properties are invariant under diffeomorphisms in [18]. Here, we select p_{chd} , instead of p_{hod} , as the variable of the obstacle avoidance navigation function².

²There is a relationship $g_{hod} = g_{chd}^{-1} g_{co}$ between p_{chd} and p_{hod} .

Firstly, we define a space D where the mobile robot can move avoiding obstacles as follows:

$$D = F - \bigcup_{i=1}^M B_i, \quad (34)$$

where $F := \{p_{chd} : \|p_{chd} - p_{c0}\|^2 \leq \rho_0^2\}$ is the mobile robot movable space which represents a Euclidean 3-dimensional disk with the center p_{c0} and the radius $\rho_0 > 0$, and $B_i := \{p_{chd} : \|p_{chd} - p_{cb_i}\|^2 < \rho_i^2\}$, $i = 1 \dots M$ denotes a M -th obstacle space in F with the center p_{cb_i} and the radius $\rho_i > 0$. We impose the additional constraint that all obstacles closures are contained in the interior of the workspace; i.e. $\|p_{cb_i} - p_{c0}\| + \rho_i < \rho_0$, $1 \leq i \leq M$, and that none of them intersect; i.e. $\|p_{cb_i} - p_{cb_j}\| > \rho_i + \rho_j$, $1 \leq i, j \leq M$. If $p_{chd} \in D$, the mobile robot keeps collision-free.

Here, we introduce the navigation function-based method as a technique for constructing artificial potential fields in order to design V_{hod}^b which can achieve the control objective. The navigation functions used in this paper are defined as follows:

Definition 1 ([11],[18]): A smooth Morse function $\varphi(p_{chd}) : D \rightarrow [0, 1]$ is a navigation function if it is

- 1) a unique minimum exists at p_{chd_f} ³;
- 2) uniformly maximal on the boundary of D .

A smooth vector field on any sphere world with a unique attractor, must have at least as many saddles as obstacles. The property of a Morse function whose Hessian at all critical points is non-degenerate establishes that the initial conditions that bring the system to saddle points are sets of measure zero. In view of this property, all initial conditions away from sets of measure zero are brought to the unique minimum [18].

In order to design the obstacle avoidance navigation function, we utilize the following function which represents the distance to the final desired relative position p_{chd_f} :

$$s(p_{chd}) = \|p_{chd} - p_{chd_f}\|^{2\kappa}, \quad (35)$$

where $\kappa > 0 \in \mathcal{R}$ is an additional parameter to change the potential field. Next, let define the obstacle function which includes the function η_0 for keeping in the space F as

$$\eta(p_{chd}) = \prod_{i=0}^M \eta_i(p_{chd}) \quad (36)$$

$$\eta_i(p_{chd}) = \begin{cases} \rho_0^2 - \|p_{chd} - p_{c0}\|^2 & \text{for } i = 0 \\ \|p_{chd} - p_{cb_i}\|^2 - \rho_i^2 & \text{for } i = 1 \dots M \end{cases}$$

Then, the model space navigation function $\tilde{\varphi}(x) \in \mathcal{R}^{2m} \rightarrow [0, 1]$ and a κ -th root function are defined as

$$\tilde{\varphi}(x) = \frac{x}{\mu + x} \quad (37)$$

and

$$\rho(x) = x^{\frac{1}{\kappa}}, \quad (38)$$

respectively, where $\mu > 0 \in \mathcal{R}$ is a parameter. The function (38) is important in order to change p_{chd_f} to a non-degenerate critical point. From Eqs. (35)–(38), the obstacle

³The position p_{chd_f} can be calculated as $g_{chd_f} = g_{co}g_{hod_f}^{-1}$. The relative pose g_{co} can be obtained by using the visual motion observer for the target object in Sec II-B.

avoidance navigation function denoted by $\varphi(p_{chd}) \in D \rightarrow \mathcal{R}$, can be developed as follows:

$$\begin{aligned} \varphi(p_{chd}) &= \rho \circ \tilde{\varphi} \circ \frac{s}{\eta}(p_{chd}) \\ &= \left(\frac{s(p_{chd})}{\mu\eta(p_{chd}) + s(p_{chd})} \right)^{\frac{1}{\kappa}} \end{aligned} \quad (39)$$

where \circ denotes the composition operator. Using a similar way in [18], it can be verified that the function (39) is the navigation function if the parameter κ is selected adequately.

D. Path Planning of Desired Body Velocity

We design the desired body velocity V_{hod}^b and the input for the estimation u_{b_i} as follows:

$$V_{hod}^b = \begin{bmatrix} -e^{-\hat{\xi}\theta_{hod}}(v_{chd}^b - \hat{p}_{hod}\omega_{chd}^b) + v_{co}^b \\ -K_{dr}e^{-\hat{\xi}\theta_{ed}}r_{ed} \end{bmatrix} \quad (40)$$

$$u_{b_i} = K_{eb}e_{b_i}, \quad (41)$$

where

$$V_{chd}^b = \begin{bmatrix} v_{chd}^b \\ \omega_{chd}^b \end{bmatrix} = \begin{bmatrix} -e^{-\hat{\xi}\theta_{chd}}K_{dp}\nabla\varphi(p_{chd}) \\ e^{\hat{\xi}\theta_{hod}}(\omega_{co}^b - \omega_{hod}^b) \end{bmatrix} \quad (42)$$

$$V_{co}^b = \begin{bmatrix} v_{co}^b \\ \omega_{co}^b \end{bmatrix} = (g_{co}^{-1}\dot{g}_{co})^\vee. \quad (43)$$

$K_{dp} := \text{diag}\{k_{dp1}, k_{dp2}, k_{dp3}\}$, $K_{dr} := \text{diag}\{k_{dr1}, k_{dr2}, k_{dr3}\}$ and $K_b := \text{diag}\{k_{b1}, \dots, k_{b6}\}$ are the positive gain matrices for the translation and the rotation of the desired body velocity and for the estimation input, respectively. $\nabla\varphi(p_{chd}) := \left(\frac{\partial\varphi(p_{chd})}{\partial p_{chd}}\right)^T$ which denotes the gradient vector of $\varphi(p_{chd})$ can be calculated as Eq. (44) at the bottom of the next page. The relative pose g_{co} can be obtained by using the visual motion observer for the target object in Sec II-B.

We are now in a position to state the main result of this paper concerning the convergence of the path planner.

Theorem 2: Suppose that $V_{wo}^b = 0$ and $V_{wb_i}^b = 0$, and the initial desired relative position $p_{chd}(0)$ satisfies $p_{chd}(0) \in D$. Then, the desired relative position $p_{chd}(t)$ ensures that $p_{chd}(t) \in D$ and $g_{hod}(t)$ has the asymptotically stable equilibrium point g_{hod_f} .

Proof: Consider the following positive definite function:

$$V_n = \varphi(p_{chd}) + \phi(e^{\hat{\xi}\theta_{ed}}) + \sum_{i=1}^M E(g_{eb_i}). \quad (45)$$

Evaluating the time derivative of V_n along the trajectories of Eqs. (27), (33), (40)–(42) gives us

$$\begin{aligned} \dot{V}_n &= (\nabla\varphi)^T \dot{p}_{chd} + r_{ed}^T e^{\hat{\xi}\theta_{ed}} \omega_{ed}^b + \sum_{i=1}^M e_{b_i}^T \text{Ad}_{(e^{\hat{\xi}\theta_{eb_i}})} V_{eb_i}^b \\ &= (\nabla\varphi)^T e^{\hat{\xi}\theta_{chd}} v_{chd}^b + r_{ed}^T e^{\hat{\xi}\theta_{ed}} \omega_{hod}^b \\ &\quad + \sum_{i=1}^M e_{b_i}^T \text{Ad}_{(e^{\hat{\xi}\theta_{eb_i}})} (-\text{Ad}_{(g_{eb_i})}^{-1} u_{b_i}) \\ &= -(\nabla\varphi)^T e^{\hat{\xi}\theta_{chd}} e^{-\hat{\xi}\theta_{chd}} K_{dp} \nabla\varphi - r_{ed}^T e^{\hat{\xi}\theta_{ed}} K_{dr} e^{-\hat{\xi}\theta_{ed}} r_{ed} \\ &\quad + \sum_{i=1}^M \left(-e_{b_i}^T K_b e_{b_i} \right) \\ &= -(\nabla\varphi)^T K_{dp} \nabla\varphi - (e^{-\hat{\xi}\theta_{ed}} r_{ed})^T K_{dr} e^{-\hat{\xi}\theta_{ed}} r_{ed} \end{aligned}$$

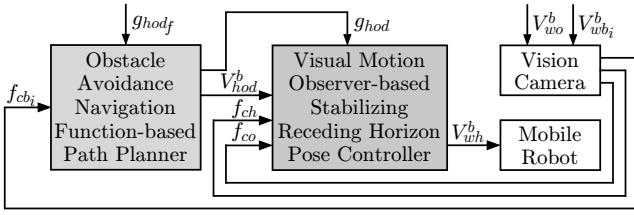


Fig. 2. Block diagram of visual motion stabilizing receding horizon control with obstacle avoidance navigation function-based path planner.

$$-\sum_{i=1}^M e_{b_i}^T K_b e_{b_i}. \quad (46)$$

It is clear from Eq. (46) that V_n is a non-increasing function in the sense that

$$V_n \leq V_n(0). \quad (47)$$

From Eqs. (45) and (47), the condition $p_{chd}(t) \in D, \forall t > 0$ is satisfied for any initial condition $p_{chd}(0) \in D$. Since the estimation error vector $e_{b_i} \rightarrow 0$, the position p_{cb_i} which is utilized in the obstacle functions converges actual value. Thanks to the property of navigation functions [18], it can be shown $p_{chd}(t) \rightarrow p_{chd_f}$ through $\nabla\varphi(p_{chd}) \rightarrow 0$. On the other hand, the rotation $e^{\hat{\xi}\theta_{cd}}(t) \rightarrow e^{\hat{\xi}\theta_{cd_f}}$ can be verified because of $e^{-\hat{\xi}\theta_{cd}} r_{cd} \rightarrow 0$. Using the relationship $g_{hod} = g_{chd}^{-1} g_{co}$, it can be concluded that $g_{hod}(t) \rightarrow g_{hod_f}$. ■

Theorem 2 guarantees the convergence of the time-varying desired pose $g_{hod}(t)$ to the final one g_{hod_f} . The path planner can be designed to keep collision-free based on the obstacle avoidance navigation function. The block diagram of the visual motion stabilizing receding horizon control with the obstacle avoidance navigation function-based path planner is shown in Fig. 2.

Our proposed approach, which deals with the estimation problem from the visual features explicitly, can be applied to 3-D visual feedback systems without restriction to the ground vehicle. Thus, the proposed method which is connected the visual motion observer-based stabilizing receding horizon control and the obstacle avoidance navigation function-based path planner without additional sensors allows us to extend technological application area. The main contribution of this paper is to provide that the path planner which can achieve obstacle avoidance during the servoing is designed for the visual feedback receding horizon control based on optimal control theory.

Remark 2: In our passivity-based visual feedback control approach, the image Jacobian-like matrix $J(\cdot)$ of the pinhole camera model is exactly the same form as that of the panoramic camera model [19]. Therefore, the proposed approach can be applied to 3-D eye-to-hand visual feedback systems with a panoramic camera using the image Jacobian-like matrix $J(\cdot)$ in [19].

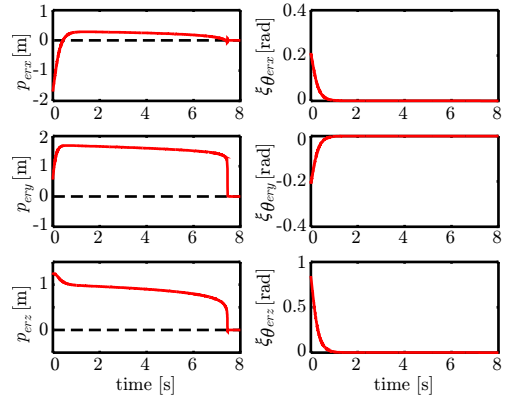


Fig. 3. Pose control error e_r .

Remark 3: Our previous work has proposed the stabilizing receding horizon control for visual feedback systems with the manipulator dynamics [9]. In a similar way, our proposed approach can be applied to robot systems which have to be controlled with a small sampling period.

V. SIMULATION RESULTS

In this section, we present simulation results for the visual feedback control with the path planner via the obstacle avoidance navigation function, compared with the constant desired relative pose proposed in [9].

Firstly, we present some results for stability analysis with the static target object and the two static obstacles. The simulation is carried out with the initial condition $p_{ho} = [-1.697 \ 0.859 \ 1.214]^T$ m, $\xi\theta_{ho} = [\pi/12 \ -\pi/12 \ \pi/3]^T$ rad. The final desired relative pose is $p_{hod_f} = [0 \ 0.3 \ 0]^T$ m, $\xi\theta_{hod_f} = [0 \ 0 \ 0]^T$ rad. The other conditions are set as $p_{co} = [0.3 \ 2 \ -2]^T$ m, $\xi\theta_{co} = [0 \ 0 \ 0]^T$ rad, $p_{cb_1} = [-0.2 \ 0.9 \ -2.75]^T$ m, $\xi\theta_{cb_1} = [0 \ 0 \ 0]^T$ rad, $\rho_1 = 0.5$ m, $p_{cb_2} = [0.75 \ 1.4 \ -2.25]^T$ m, $\xi\theta_{cb_2} = [0 \ 0 \ 0]^T$ rad, $\rho_2 = 0.5$ m. To solve the real time optimization problem, the software C/GMRES [20] is utilized. The control input with the receding horizon control is updated every 10 ms. It must be calculated by the receding horizon controller within that period. The horizon was selected as $T = 0.01$ s.

The simulation results for the static obstacles are presented in Figs. 3 and 4 and Table I. Fig. 3 shows the actual pose control error e_r , which is the error vector between the current relative pose $g_{ho}(t)$ and the final desired one g_{hod_f} . The asymptotic stability can be confirmed by steady state performance in Fig. 3.

Fig. 4 presents the trajectory of the position of the mobile robot p_{wh} . In Fig. 4, the spheres and the cube show the static obstacles and target object, respectively. The solid (red) lines denote the trajectory applying the proposed stabilizing receding horizon control with the path planner, and the dashed (blue) lines denote those with the constant desired

$$\nabla\varphi(p_{chd}) = \frac{2\mu}{\kappa(\mu\eta + s)^{\frac{1+\kappa}{\kappa}}} \left(\kappa\eta(p_{chd} - p_{chd_f}) + \|p_{chd} - p_{chd_f}\|^2 \left(\prod_{i=1}^M \eta_i(p_{chd} - p_{co}) - \sum_{j=1}^M \prod_{i=0, i \neq j}^M \eta_i(p_{chd} - p_{cb_j}) \right) \right) \quad (44)$$

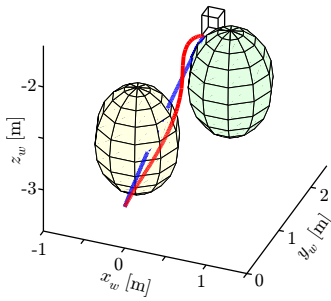


Fig. 4. Trajectory of position p_{wh} with static obstacles: Solid (Red); applying proposed method: Dashed (Blue); applying previous one [9].

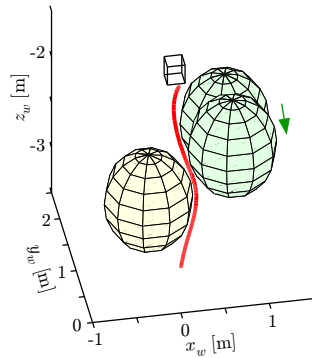


Fig. 5. Trajectory of position p_{wh} with moving obstacle

TABLE I
VALUES OF THE COST FUNCTION.

Control Scheme	cost
Feedback Control without Optimization	0.557
Receding Horizon Control ($T = 0.01$ s)	0.409
Receding Horizon Control ($T = 0.1$ s)	0.180
Receding Horizon Control ($T = 1$ s)	0.057

value. The trajectory should be designed that the mobile robot moves toward the cube avoiding the spheres. From Fig. 4, it is concluded that the proposed method can make the mobile robot avoid all obstacles. Although the convergence to the desired values is also achieved in the case of the previous method [9] in the simulation, it corresponds to fail in the actual experiment since the mobile robot hits the obstacles.

Subsequently, the performance for the stabilizing receding horizon control is compared in terms of the integral cost in Table I. The cost is calculated by the following function:

$$Cost = \int_0^8 l(x(\tau), u(\tau)) d\tau. \quad (48)$$

Since the cost of the stabilizing receding horizon method is smaller than the previous method without optimal control theory [8] under conditions of the adequate cost function, it can be easily verified that the control performance is improved. In addition, the cost is reduced as the horizon length increases from $T = 0.01$ to $T = 1$.

Next, we perform the simulation with the moving obstacle. Although one of the assumptions of Theorem 2, i.e., $V_{wb_i}^b = 0$, is not satisfied in the case of the moving obstacle, we also validate the effectiveness of the proposed method from a practical point of view. The condition of the obstacle 2 changes to $p_{cb_2} = [0.75 \ 1.4 - 0.05t - 2.25]^T$ m from the aforementioned one. The simulation results for the moving obstacle are presented in Fig. 5. From Fig. 5, the path planner generates the reference trajectory avoiding the obstacle and the mobile robot follows the generated trajectory. This result leads to the consideration that the proposed control scheme would be useful in the case of the moving obstacle.

VI. CONCLUSIONS

This paper proposes stabilizing receding horizon control via an obstacle avoidance navigation function for 3-D eye-

to-hand visual feedback systems, which are highly nonlinear and relatively fast systems. The main contribution of this paper is to show that the path planner which can avoid obstacles during servoing is designed for the visual feedback receding horizon control based on optimal control theory. Simulation results are presented to verify the control performance with obstacle avoidance of the proposed control scheme.

REFERENCES

- [1] F. Chaumette and S. A. Hutchinson, "Visual Servoing and Visual Tracking," In: B. Siciliano and O. Khatib (Eds.), *Springer Handbook of Robotics*, Springer-Verlag, pp. 563–583, 2008.
- [2] V. Lippiello, B. Siciliano and L. Villani, "Position-based Visual Servoing in Industrial Multirobot Cells using a Hybrid Camera Configuration," *IEEE Trans. on Robotics*, Vol. 23, No. 1, pp. 73–86, 2007.
- [3] N. R. Gans and S. A. Hutchinson, "Stable Visual Servoing through Hybrid Switched-System Control," *IEEE Trans. on Robotics*, Vol. 23, No. 3, pp. 530–540, 2007.
- [4] J. P. Swensen, V. Kallem and N. J. Cowan, "Empirical Characterization of Convergence Properties for Kernel-based Visual Servoing," In: G. Chesi and K. Hashimoto (Eds.), *Visual Servoing via Advanced Numerical Methods*, Springer-Verlag, pp. 22–38, 2010.
- [5] G. Allibert, E. Courtial and F. Chaumette, "Predictive Control for Constrained Image-based Visual Servoing," *IEEE Trans. on Robotics*, Vol. 26, No. 5, pp. 933–939, 2010.
- [6] N. R. Gans, G. Hu, K. Nagarajan and W. E. Dixon, "Keeping Multiple Moving Targets in the Field of View of a Mobile Camera," *IEEE Trans. Robotics*, Vol. 27, No. 4, pp. 822–828, 2011.
- [7] H. Kawai, T. Murao and M. Fujita, "Passivity-based Dynamic Visual Feedback Control with Uncertainty of Camera Coordinate Frame," *Proc. of the 2005 American Control Conference* pp. 3701–3706, 2005.
- [8] M. Fujita, H. Kawai and M. W. Spong, "Passivity-based Dynamic Visual Feedback Control for Three Dimensional Target Tracking: Stability and L_2 -gain Performance Analysis," *IEEE Trans. on Control Systems Technology*, Vol. 15, No. 1, pp. 40–52, 2007.
- [9] T. Murao, H. Kawai and M. Fujita, "Predictive Visual Feedback Control with Eye-in/to-Hand Configuration via Stabilizing Receding Horizon Approach," *Proc. of the 17th IFAC World Congress on Automatic Control*, pp. 5341–5346, 2008.
- [10] J. Minguez, F. Lamiroux and J.-P. Laumond, "Motion Planning and Obstacle Avoidance," In: B. Siciliano and O. Khatib (Eds.), *Springer Handbook of Robotics*, Springer-Verlag, pp. 827–852, 2008.
- [11] E. Rimon and D. E. Koditschek, "Exact Robot Navigation using Artificial Potential Functions," *IEEE Trans. Robotics and Automation*, Vol. 8, No. 5, pp. 501–518, 1992.
- [12] N. J. Cowan, J. D. Weingarten and D. E. Koditschek, "Visual Servoing via Navigation Functions," *IEEE Trans. Robotics and Automation*, Vol. 18, No. 4, pp. 521–533, 2002.
- [13] J. Chen, D. M. Dawson, W. E. Dixon and V. K. Chitrakaran, "Navigation Function-based Visual Servo Control," *Automatica*, Vol. 43, No. 7, pp. 1165–1177, 2007.
- [14] T. Murao, H. Kawai and M. Fujita, "Visual Motion Observer-based Stabilizing Receding Horizon Control via Image Space Navigation Function," *Proc. of the 2010 IEEE Multi-conference on Systems and Control*, pp. 1648–1653, 2010.
- [15] W. H. Huang, B. R. Fajen, J. R. Fink and W. H. Warren, "Visual Navigation and Obstacle Avoidance using a Steering Potential Function," *Robotics and Autonomous Systems*, Vol. 54, No. 4, pp. 288–299, 2006.
- [16] A. Cherubini and F. Chaumette, "Visual Navigation with Obstacle Avoidance," *Proc. 2011 IEEE/RSJ International Conference on Intelligent Robots and Systems*, pp. 1593–1598, 2011.
- [17] R. Murray, Z. Li and S. S. Sastry, *A Mathematical Introduction to Robotic Manipulation*, CRC Press, 1994.
- [18] D. E. Koditschek and E. Rimon, "Robot Navigation Functions on Manifolds with Boundary," *Advances in Applied Mathematics*, Vol. 11, No. 4, pp. 412–442, 1990.
- [19] H. Kawai, T. Murao and M. Fujita, "Passivity-based Visual Motion Observer with Panoramic Camera for Pose Control," *Journal of Intelligent and Robotic Systems*, Vol. 64, No. 3–4, pp. 561–583, 2011.
- [20] T. Ohtsuka, "A Continuation/GMRES Method for Fast Computation of Nonlinear Receding Horizon Control," *Automatica*, Vol. 40, No. 4, pp. 563–574, 2004.